SAND2018-4422J

A 7.2 keV spherical x-ray crystal backlighter for two-frame, two-color backlighting at Sandia's Z Pulsed Power Facility

M.S. Schollmeier,[1, a)] P.F. Knapp,[1] D.J. Ampleford,[1] E.C. Harding,[1] C.A. Jennings,[1] D.C. Lamppa,[1] G.P. Loisel,[1] M.R. Martin,[1] G.K. Robertson,[1] J.E. Shores,[1] I.C. Smith,[1] C.S. Speas,[1] M.R. Weis,[1] J.L. Porter,[1] and R.D. McBride[1, 2]

[1)] *Sandia National Laboratories, Albuquerque, NM 87185, USA*

[2)] *University of Michigan, Nuclear Engineering and Radiological Sciences Department, Ann Arbor, MI, United States*

Many experiments on Sandia National Laboratories' Z Pulsed Power Facility — a 30 MA, 100 ns rise-time, pulsed-power driver — use a monochromatic quartz crystal backlighter system at 1.865 keV (Si He_α) or 6.151 keV (Mn He_α) x-ray energy to radiograph an imploding liner (cylindrical tube) or wire array z-pinch. The x-ray source is generated by the Z-Beamlet Laser (ZBL), which provides two, 527-nm, 1 kJ, 1-ns laser pulses. Radiographs of imploding, thick-walled Beryllium liners at convergence ratios C_R above 15 [$C_R = r_\mathrm{i}(0)/r_\mathrm{i}(t)$] using the 6.151-keV backlighter system were too opaque to identify the inner radius r_i of the liner with high confidence, demonstrating the need for a higher-energy x-ray radiography system. Here, we present a 7.242 keV backlighter system using a Ge(335) spherical crystal with the Co He_α resonance line. This system operates at an almost identical Bragg angle as the existing 1.865 keV and 6.151 keV backlighters, enhancing our capabilities for two-color, two-frame radiography without modifying the system integration at Z. The first data taken at Z include nearly simultaneous 6.2-keV and 7.2-keV two-color radiographs as well as radiographs of low-convergence ($C_R \approx 4 - 5$), large-diameter liner implosions.

[a)] Electronic mail: mscholl@sandia.gov

I. INTRODUCTION

For more than three decades, spherical-crystal based, monochromatic x-ray backlighter radiography[1–8] has been an essential probe for high-energy density physics (HEDP) experiments. Bent-crystal microscopes can provide high spatial resolution over a cm-size field of view. They operate within a narrow spectral bandwidth ($\Delta E/E \approx 10^{-3} - 10^{-4}$), which results in nearly monochromatic images that allow for an easier interpretation compared to broad- band images, for example, from point-projection backlighter systems.
For the last eight years, the majority of experiments at Sandia's Z Pulsed Power Facility ("Z")[9] studying inertial confinement fusion used the immense magnetic pressure generated by Z to implode empty, gas- or liquid-filled, hollow Be cylinders (liners) for studies of, for example, the Magneto-Rayleigh-Taylor instability without[10,11] or with pre-imposed axial magnetic field[12,13], or the electrothermal instability[14,15]. Understanding and mitigating these instabilities is important for the Magnetized Liner Inertial Fusion (MagLIF) concept[16,17], where fusion fuel is magnetized with an external field coil, preheated with a multi-kJ laser pulse, and compressed using Z to achieve thermonuclear conditions[18].

In a typical backlighter experiment as shown in Fig. 1, the 527-nm, 1-kJ, 1-ns Z-Beamlet Laser (ZBL)[19] is used to generate a plasma x-ray source. ZBL provides two spatially and temporally separated foci in the Z target chamber, enabling two-frame imaging with an inter-frame time range of 2-20 ns[20].

The spherical-crystal imaging system at Z consists of either two quartz (1 0 1) crystals using the 1.865 keV Si He$_\alpha$ emission line, or two quartz (2 2 3) crystals using the 6.151 keV Mn He$_\alpha$ intercombination line[21]. Note that we omit the conjugate plane in the designation of the Miller indices for quartz crystals (e.g., quartz $(2\,2\,\bar{4}\,3)$ becomes quartz (2 2 3)) for consistency with the other crystals mentioned here. The backlighter systems operate at a magnification of 5.8, using crystals with $R = 250\,\mathrm{mm}$ radius of curvature. X-rays emitted from the two sources penetrate the imploding liner at the center of Z, are reflected and focused by the two crystals, pass through two return apertures for debris and background mitigation, and are then detected with image plate detectors. The large amount of debris generated in a Z experiment requires significant shielding of the detectors, which are placed inside of a 1-inch tungsten enclosure (the "backlighter camera").

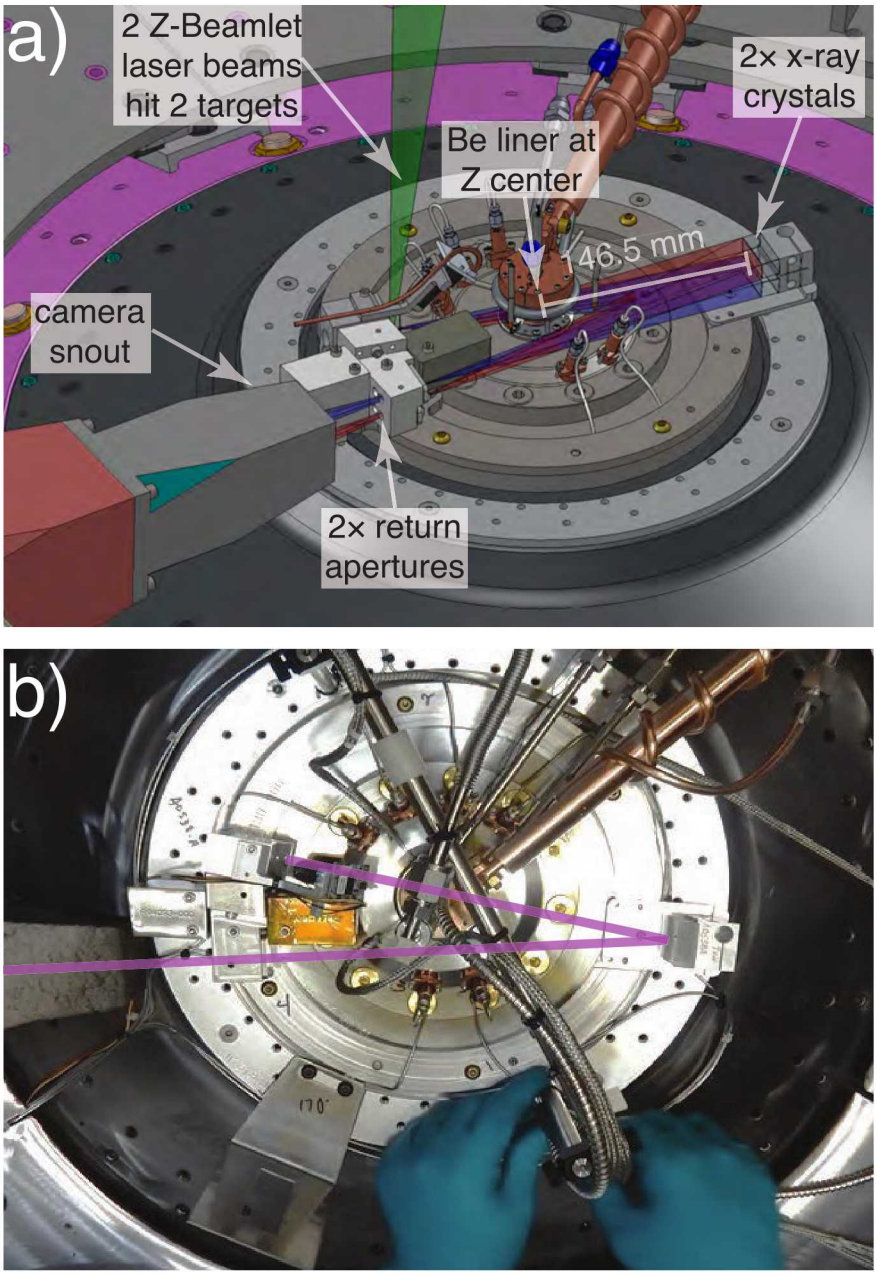

FIG. 1. Typical backlighter setup at the Z Pulsed Power Facility. a) shows a computer aided design model of the Z center section, with a Be liner hidden inside the return current can and the backlighter mounted on a ring. The ZBL laser generates two pulses that irradiate two separate targets. Two identical crystals mounted on top of each other reflect and image x-rays propagating through the liner to a set of return apertures. Behind the apertures is the snout of the detector shielding enclosure ("backlighter camera"). b) shows a photograph of the experiment at Z. For spatial reference, a technician's hands can be seen assembling some parts.

While the x-ray optical design or crystal dimensions stayed unchanged since 2008[20], the crystal mounting hardware and its alignment precision was improved in 2013[22] after identifying potential issues due to movement of the crystal between alignment and downline shot. The design was changed from an assembly of commercial miniature stages to a monolithic Al block with flexure arms and locking setscrew combination to adjust only tip and tilt of the crystal while the distance to the liner stays fixed, see Fig. 1a.

For implosions at high convergence ratio $C_R > 15$, where $C_R = r_i(0)/r_i(t)$ and r_i the inner radius of the liner, the Be liners become too opaque for 6 keV x-rays to determine the position of the inner radius $r_{\rm i}(t)$ with high confidence. Hence, a backlighter system with higher x-ray energy was required. Design requirements were that it performs similar to or better than the 6 keV system in terms of image brightness, spatial resolution, and Bragg angle which affects astigmatism. In the following sections, we describe these requirements in more detail, determine potential candidates for above-6-keV backlighting, present the chosen 7.2 keV backlighter system as well as laser-only tests to determine image brightness and spatial resolution, and finally we show examples of 7.2 keV radiographs at the Z Pulsed Power Facility.

II. DESIGN REQUIREMENTS

A. Liner transmission

When the liner converges radially during the Z implosion, its density increases. High-quality compressions require a stable (straight) inner wall during the implosion to reach high stagnation pressures and temperatures. The trajectory and integrity of the inner wall are experimentally measured by taking x-ray radiographs at various stages during the implosion, which requires that the liner is partially transparent for the probe x-rays. Assuming a perfect, cold compression without any mass losses, the density ρ of a cylindrical liner with inner radius r_i and wall thickness d depends on the convergence ratio as

$$\rho(C_R) = \rho_0\, C_R \frac{(r_i + d)^2 - r_i^2}{(r_i + C_R\, d)^2 - r_i^2}. \tag{1}$$

The strongest absorption of x-rays penetrating the liner occurs along the inner wall surface. This limb thickness is a function of C_R as well, and can be calculated as

$$L(C_R) = \frac{2}{C_R}\left[(r_i + C_R\, d)^2 - r_i^2\right]^{1/2}. \tag{2}$$

Both Eq. (1)and Eq. (2) are used to calculate the limb transmission according to the Beer-Lambert law $T = \exp(-\mu\rho L)$, where μ denotes the mass attenuation coefficient. Here we use cold, solid density values for simplicity.

Fig. 2a shows the limb transmission vs. C_R for a Be liner with $r_i = 3.44\,\mathrm{mm}$ and $d = 0.4\,\mathrm{mm}$. The plots show the limb transmission scaling for five different x-ray emission lines from He-like ions or cold K_α lines. The limb transmission decreases strongly with increasing C_R for x-ray energies below 10 keV. Above 10 keV, the transmission stays high even at $C_R = 20$. A limb transmission of about 50% yields an optimum contrast and requires x-ray energies near or above 10 keV. However, both the ZBL laser conversion efficiency into x-rays (see Fig. 10 in Ref.[19]) as well as the integrated reflectivity of any suitable crystals[23] quickly drop with increasing x-ray energy, rendering sources near or above 10 keV unusable with the present capabilities.

The limb transmission for the 6.151 keV Mn He_α x-ray backlighter system is below 5% for $C_R > 5$ (see Fig. Fig. 2b), which can complicate the interpretation of experimental radiographs as the measurement of the inner radius suffers from a poor signal-to-noise ratio. Increasing the backlighter energy by only one (two) keV, which corresponds to an increase of 17% (30%) relative x-ray energy, increases the transmission by about five (ten) times. This is a significant improvement in transmission for a modest change in x-ray energy.

The idealized calculations from above are corroborated by synthetic radiographs from a 3D resistive-MHD GORGON simulation[24] of an imploding liner at Z. This simulation imploded a MagLIF-scale Beryllium liner with $r_i = 2.325$ mm and $d = 0.465\,\mathrm{mm}$[18], but used a liquid deuterium fill to reduce the final convergence achieved. Note that the initial inner radius and wall thickness are slightly different to the Be liner used in the analytical example above. This target stagnates at larger radii compared to a high-convergence MagLIF target, since it was intended to be more easily diagnosed with radiography. Fig. 3 shows a density slice at peak compression (an inner surface convergence of $C_R = 12$ resulting in a $400\,\mu\mathrm{m}$ inner diameter), as well as synthetic radiographs for 6, 7.2 or 10 keV x-rays. Fig. 4 shows axially averaged lineouts of the transmission images. Similar to Fig. 2, the liner is opaque

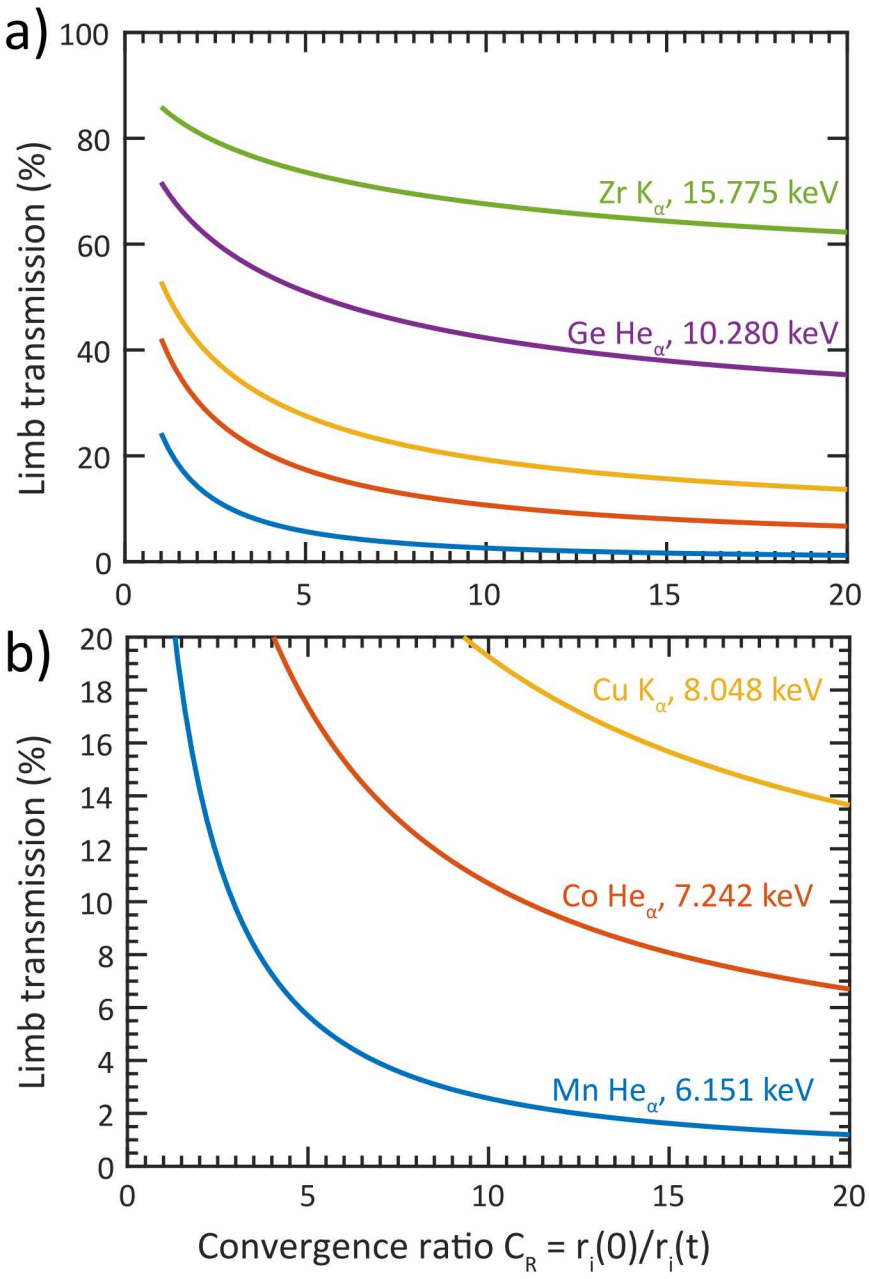

FIG. 2. Limb transmission of a Be liner vs. convergence ratio C_R and x-ray energy. a) For x-rays below 10 keV, the transmission drops quickly when the liner converges. Above 10 keV the transmission stays relatively constant. As shown in b), increasing the x-ray backlighter energy by one or two keV compared to the standard 6 keV system increases the transmission significantly, even for high convergence ratios near 20.

for 6 keV x-rays with a limb transmission of less than 1%. At 7.2 keV the limb transmission is about 4%, sufficient to locate the inner surface. This further indicates that raising the x-ray backlighter energy by 1 keV or more will lead to significant contrast enhancement. At 10 keV energy the transmission retains at about 27%, however as mentioned above, a 10 keV x-ray backlighter system is currently not attainable at our facility.

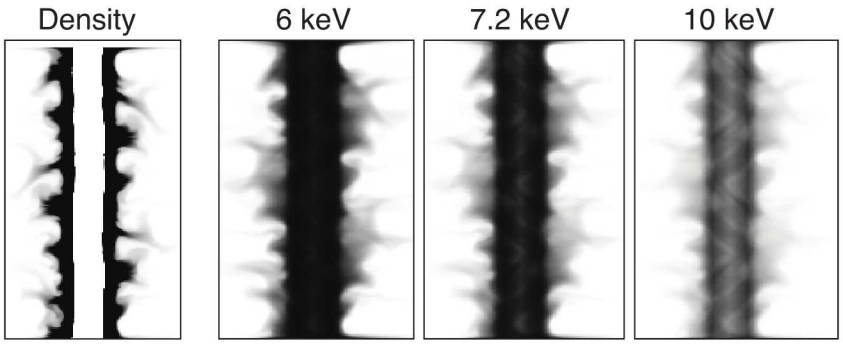

FIG. 3. Synthetic radiographs of a liquid deuterium-filled, imploding liner at the Z facility. The left image shows a density slice at peak compression with $C_R = 12$, the three right images show synthetic radiographs at 6, 7.2, and 10 keV energy.

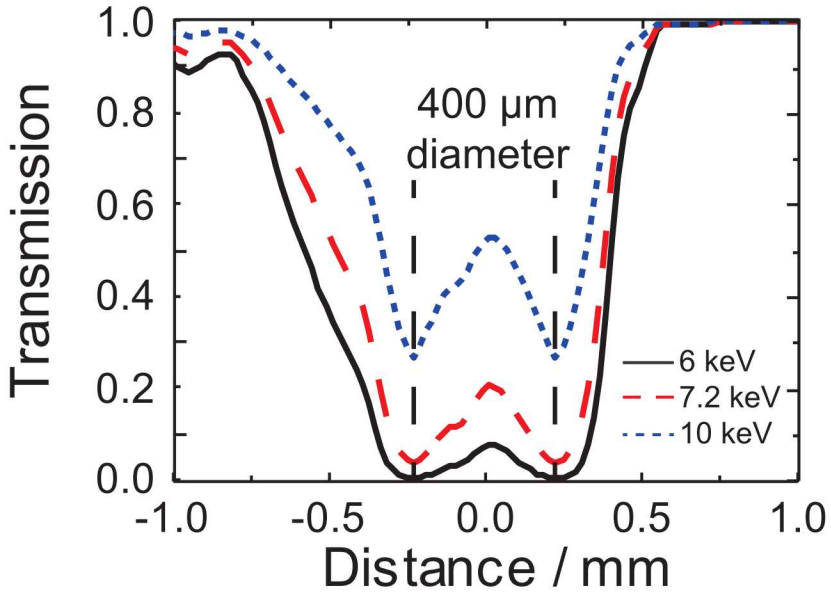

FIG. 4. Transmission of the synthetic radiographs from Fig. 3. Min. transmission for 10 keV retains 27%, 7 keV retains 4%, and 6 keV retains <1%.

B. Bragg angle and system integration at Z

Another design requirement for a higher-energy backlighter system at Z was to keep the Bragg angle of the new system close to 83°, which is close to the Bragg angles of the existing 1.865 and 6.151 keV systems and allows for two-color imaging (using two different sources and crystals) with ZBL[20]. It also simplifies the testing of the new system during downline shots at Z because one frame can be used with the reliable 6.2 keV system while the other frame can be used to test the new system without risking a complete data loss if the new system experiences issues.

Another reason to keep the Bragg angle close to the existing system is the integration at Z. The liner is always at the Z center, which means that a new backlighter system with an angle different than 83° needs the detector (and x-ray source) at a different position. Fig. 5 shows a computer aided design model of the backlighter camera sitting on top of the cover plates of the magnetically insulated transmission lines (MITL). The camera housing can accommodate two 75-mm long image plate detectors and has room for a future upgrade with a time-gated detector. The housing is made out of 1" tungsten plates for debris and background protection, weighs about 400 kg, and can only be moved with a crane. The MITL plates have dedicated cutouts for the camera, which restricts camera positioning. Furthermore, the camera snout reaches into the blast shield that is used to contain debris created following the liner implosion, and hence the blast shield needs to be specifically designed for the camera. In the case of MagLIF, the the superstructure that surrounds the target and is used to separate the magnetic field coils[25] has specific slots cut into this structure for both the incident and reflected x-ray backlighter paths. Another important constraint is the return current can, which limits the Bragg angle to less than 86° for the current MagLIF geometry.

The hardware on Z could have been modified for a new backlighter system if absolutely needed, but this would have required significant engineering efforts. However, in the following section we show that re-engineering was not needed since promising imaging systems near 83° could be identified.

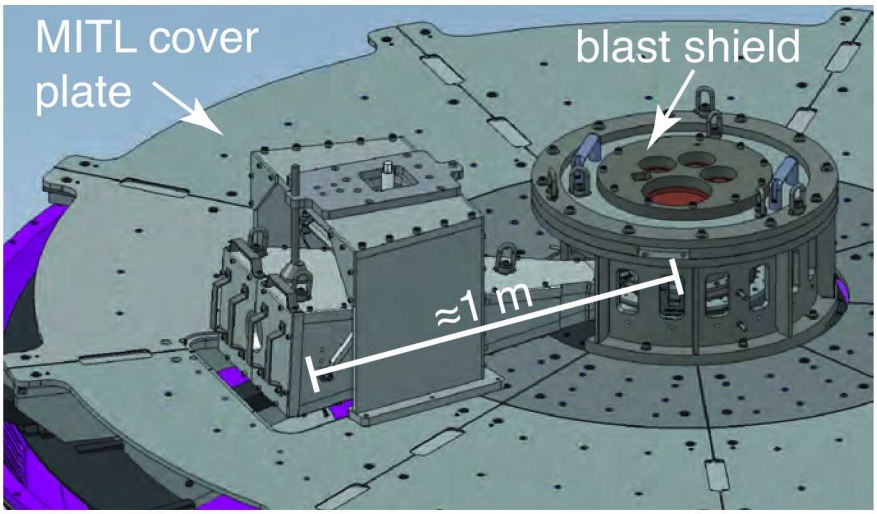

FIG. 5. Computer aided design model of the backlighter camera and blast shield sitting on top of the MITL cover plates at Z. The size and weight (about 400 kg) of the camera constrains the backlighter system integration at Z to a small range of possible Bragg angles.

C. Image brightness, magnification and spatial resolution

A typical backlighter shot uses two 1-kJ, 1-ns ZBL pulses at 527 nm, each of which have a conversion efficiency of about $(1-2)\times10^{-3}$ into the Mn He_α line complex[19,26]. At keV plasma temperatures, most of the He_α emission is either in the resonance ($1s\,2p\,^1P_1 \rightarrow 1s^2\,^1S_0$) or intercombination ($1s\,2p\,^3P_1 \rightarrow 1s^2\,^1S_0$) lines of the spectrum. Hence, the conversion efficiency into the 6.151 keV Mn intercombination line is estimated to be about 5×10^{-4}, which corresponds to 5×10^{14} 6.151-keV photons emitted from each source. This backlighter configuration generates images with a brightness of about 2 photons per $\mu\mathrm{m}^2$, with a detector-limited resolution of about $12\,\mu\mathrm{m}$ in the object plane[27]. A requirement for the higher-energy backlighter system was that the new system should generate images with similar magnification, resolution and image brightness as the existing 6.151-keV system.

III. SPHERICAL CRYSTAL IMAGING SYSTEMS FOR $(83\pm1)^\circ$

Suitable x-ray crystal and spectral-line combinations were taken from Ref.[23]. The range of Bragg angles was restricted to $(83\pm1)^\circ$ to fulfill the Bragg angle requirements mentioned above. The list of spectral lines was limited to the He-like resonance and intercombination lines for the elements Si to Ge, since these lines can be efficiently generated with ZBL. The

best candidates are presented in Tab. I. For each match, we show the source element, line energy, crystal material with corresponding Miller indices ($h\,k\,l$) and $2d$ lattice spacings, as well as the Bragg angle and integrated reflectivity R_{int}. The integrated reflectivity was calculated with XOP's[28] multi-lamellar model for a bent crystal with 250 mm radius and 70 μm thickness. Knowledge of the ZBL laser energy to x-ray energy conversion efficiency[19,26] lets us calculate the expected image brightness for a ZBL-backlighter system with magnification of six[27]. These results are listed in the last column of Tab. I.

TABLE I. Most efficient spectral line and crystal matches for Bragg angles of $\vartheta_B = (83 \pm 1)^\circ$ for x-ray source elements from Si to Ge (2-10 keV). The integrated reflectivity was calculated with XOP[28] using the multi-lamellar model for a bent crystal with 250 mm radius of curvature and 70 μm thickness. The image brightness was calculated using Z-Beamlet x-ray conversion parameters, a magnification of six and for a detector with 25 μm pixel size.

element	energy [keV]	crystal	Miller indices (hkl)	$2d$ spacing [Å]	ϑ_B [°]	R_{int} [μrad]	Image brightness [Photons/pixel]
14 Si	1.865	quartz	(1 0 1)	6.6863	83.9	185.40	56000
17 Cl	2.789	quartz	(1 1 1)	4.4727	83.5	64.93	8500
18 Ar	3.124	Ge	(2 2 0)	4.0004	82.8	843.15	130000
20 Ca	3.883	quartz	(1 2 0)	3.2163	83.1	11.25	900
21 Sc	4.295	quartz	(1 1 3)	2.9055	83.5	52.98	2900
25 Mn	6.151	quartz	(2 2 3)	2.0297	83.2	85.98	1250
27 Co	7.242	Ge	(3 3 5)	1.7255	82.8	118.6	625
28 Ni	7.766	quartz	(2 4 0)	1.6082	83.1	63.32	350
30 Zn	8.999	InAs	(1 5 7)	1.39395	83.6	69.5	180
31 Ga	9.628	quartz	(1 6 0)	1.2977	82.9	26.48	27
32 Ge	10.280	Si	(8 4 0)	1.2143	83.3	62.12	45

The table shows that the already-used 1.865 and 6.151 keV backlighter systems are indeed the most efficient combinations for their respective energy. The overall most efficient crystal is Ge (2 2 0) with $R_{\mathrm{int}} = 843.15\,\mu$rad in combination with the Ar intercombination line at 3.124 keV. While Ar cannot be easily used as a ZBL laser target, this crystal is used for

self-emission imaging of the imploding liner at Z[18] . Above 6.151 keV, the image brightness for matching combinations quickly approaches only a few photons per pixel. The highest image brightness for a working combination above 6.151 keV is the Co resonance line at 7.242 keV with a Ge (3 3 5) crystal. The expected image brightness at 7.2 keV is two times lower than at 6.2 keV, which would still be acceptable. If the image brightness is too low, the x-ray source can be moved 31.6 mm inside the Rowland circle to increase the image brightness about twofold at the cost of field of view[3].

IV. LASER-ONLY TESTS

Before fielding the 7.2 keV backlighter system on Z, the crystals were tested in one of the target chambers at the Z-Backlighter facility[19]. ZBL was used in single-frame configuration, delivering 1 to 1.5 kJ in a 1-ns pulse. A 0.5-ns, 100-J picket preceded the main pulse by 3.5 ns to enhance the x-ray yield[29]. The laser was focused onto 25-μm thick Co foils to generate the 7.242 keV characteristic line radiation. A spherical Ge (3 3 5) crystal with $R = 250\,\mathrm{mm}$ and rectangular aperture (28 mm meridional, 10 mm sagittal) was set up in a backlighter configuration with the x-ray source on the Rowland circle. Both a static, 150 lines-per-inch (lpi) W mesh and a 0.5-mm-thick W knife edge served as radiography objects, placed at a distance of 146.6 mm from the crystal. A filtered Fuji TR image plate was used as the detector, placed at 850 mm from the crystal to yield a magnification of 5.8, identical to the 6.151-keV backlighter system[20]. Since the crystal aperture is identical to the aperture of the 6.151-keV crystals, the field of view of $11.4 \times 4.1\,\mathrm{mm}^2$ is also identical.

The W mesh was used to verify the magnification and, in the unobstructed areas, the flatfield homogeneity. The knife edge was used to infer the spatial resolution of the combined image plate plus crystal imaging system. Multiple shots were taken with the knife in either horizontal or vertical direction to measure the resolution in both the sagittal and meridional directions. The image plates were scanned with a Fuji FLA7000 scanner with $25 \times 25\,\mu\mathrm{m}^2$ pixel size; the data were corrected for fading using our own calibration curve. Fig. 6a shows a magnified view of the mesh wires and the tungsten knife edge, which covers the right half of the image. The red box marks the area taken to infer the edge spread function (ESF) 10%-90% width, which is used here to determine the spatial resolution of the system. Fig. 6b shows the lineout of the data, together with a fit assuming a Gaussian line spread function.

The measured data were further compared to ray-tracing simulations using the code described in Ref.[27]. The simulations used the as-fielded distances. The source photon yield was calculated from the laser energy using conversion efficiencies measured earlier[19,26]. The rocking curve was imported into the simulation from an XOP data table. The simulated detector had 25 μm pixel size; the image was post-processed using a 65-μm Gaussian point spread function[30] to simulate the IP resolution.

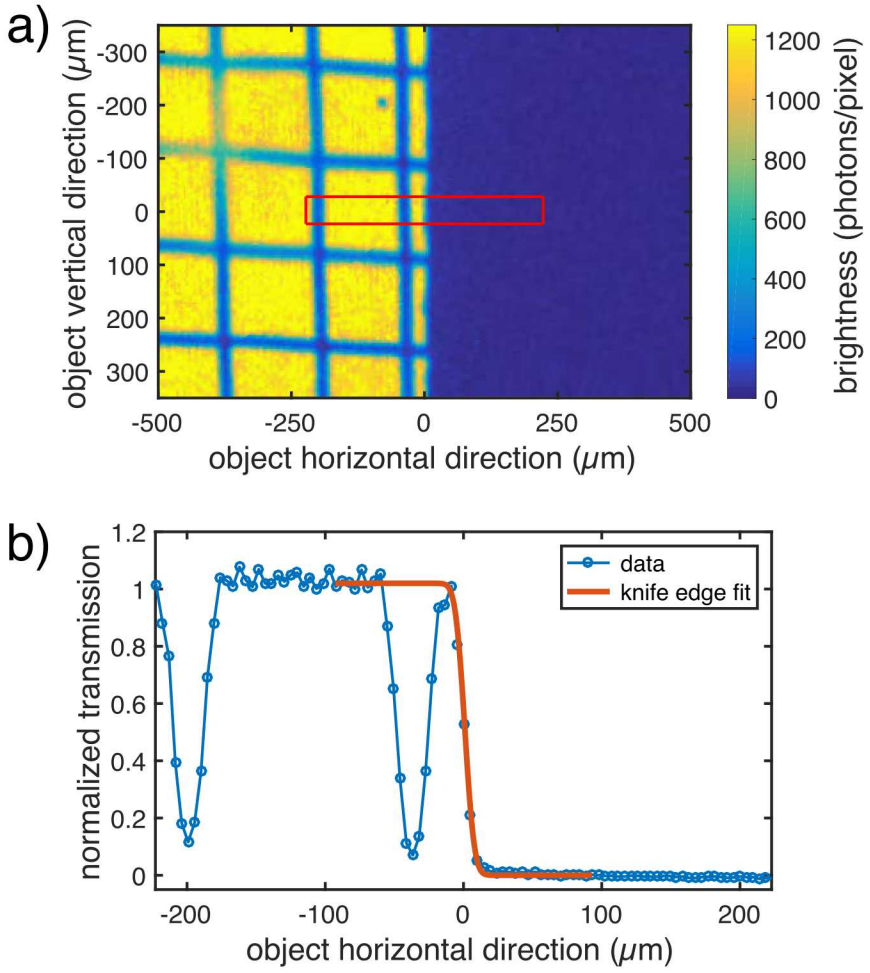

FIG. 6. Laser-only tests demonstrated the feasibility of using Ge (335) for radiography. a) shows a magnified view of the image plate detector showing the 150-lpi W mesh and W knife edge to the right. b) shows the edge spread function, obtained by averaging the area shown in the red box in a), compared to a fit assuming a Gaussian line spread function.

Tab. II shows the simulated ESF widths and image brightness, compared to the measurements. Due to astigmatism, the sagittal and meridional ESFs are different; the resolution

of this backlighter system is slightly better in the meridional (radial on Z) direction. The ray-tracing simulations assume a perfect crystal with zero surface defects, which for a perfect detector results in better resolution than measured[27]. The image plate detector limits the system spatial resolution, as in the 6.151-keV backlighter system. However, the comparison to the ray-tracing model shows that the Ge crystal is of high quality and does not degrade the spatial resolution.

The comparison of the simulated and measured image brightness shows that the real system is about a factor of two brighter than anticipated. The error quoted for the experimental data represents the minimum/maximum shot-to-shot variation of the measurements, normalized to 1 kJ laser energy. The exact origin of the discrepancy between model and experiment is currently not known. Calculating the expected image brightness depends on many parameters that are not well benchmarked: the conversion efficiency of laser into a single spectral line is not well known and had to be estimated, furthermore the calculated crystal reflectivity could also be wrong by some factor. As stated in[23], the crystal reflectivity in these calculations is strongly affected by the temperature (Debye-Waller) factor. In most cases a temperature factor between 0.8 and 0.9 yields satisfying results; a lower temperature factor results in a lower integrated reflectivity. Here, a factor of 0.8 was chosen, which may underestimate the reflection efficiency.

TABLE II. Comparison of image brightness and spatial resolution vs. ray-tracing simulations. The experimental data were obtained in laser-only shots at the Z-Backlighter facility using a Co target, Ge (3 3 5) crystal with 250 mm radius of curvature, and magnification of 6. The edge spread function (ESF) width is measured at the 10% and 90% points. The pixel size of the image is $25 \times 25\,\mu\mathrm{m}^2$.

Quantity	Ray-tracing model	Experimental data
Meridional ESF width [μm]	12 ± 1	12.5 ± 0.5
Sagittal ESF width [μm]	15 ± 1	16 ± 0.5
Brightness [phot./px]	750	1280 ± 250

V. DYNAMIC RADIOGRAPHS AT THE Z FACILITY

After confirming with laser-only shots that the 7.2-keV backlighter meets the requirements, the system was fielded at Z. The first integrated Z shots testing this new capability fielded the 6.2-keV backlighter for the first frame and the new 7.2-keV backlighter for the second frame during an early time of the implosion. The two-color configuration was selected for a direct comparison of both systems in a dynamic radiography experiment, and to reduce the risk for data loss for the case that the 7.2-keV system does not produce an image. Fig. 7a shows the two radiographs obtained for an imploding liner with 'thick ends' (the two bulges top left and right)[31]. The left radiograph was taken with the 6.151-keV backlighter, the right radiograph was taken 5 ns later with 7.242 keV. Fig. 7b shows a lineout of the area marked by the red lines in a). The top of the radiographs feature a shadow of the top Helmholtz B-field coil on top of the liner[25]. In this experiment, the limb transmission of the 7.2-keV x-rays is about a factor of three better than the 6.2-keV transmission and the 7.2-keV image shows a better contrast in this area than the 6.2-keV image. A darker feature appears in both images right at the inner wall of the liner at $r \approx 2.3\,\mathrm{mm}$, which shows up in the lineouts as a small dip with higher absorption. This feature is from a sub-100-nm, high-opacity Pt coating that was vapor-deposited at the inner wall to locally enhance radiographic contrast (see Ref.[12] for a detailed discussion of the radiographic tracer-layer technique).

A. Influence of fringe magnetic fields

An examination of the object-free image area in Fig. 7a for radii greater than 3 mm reveals a gradient in the top-down direction of the 7.2-keV image, which is absent in the 6.2-keV image. A second set of two-color radiographs in another Z shot also showed a homogeneous flat field for 6.2-keV x-rays but again a vertical gradient in the 7.2-keV image, as well as a much dimmer exposure indicating an alignment issue with the 7.2-keV system. A vertical gradient in the backlighter image cannot be created by misalignment of the Bragg angle, which would result in a horizontal gradient. A vertical gradient can be created by partial clipping of the x-ray beam after the crystal reflection, for example at the 3-mm diameter return aperture. However, a pointing error of the reflected x-ray beam could be ruled out because the image was centered at the image plate detector. These observations suggest that

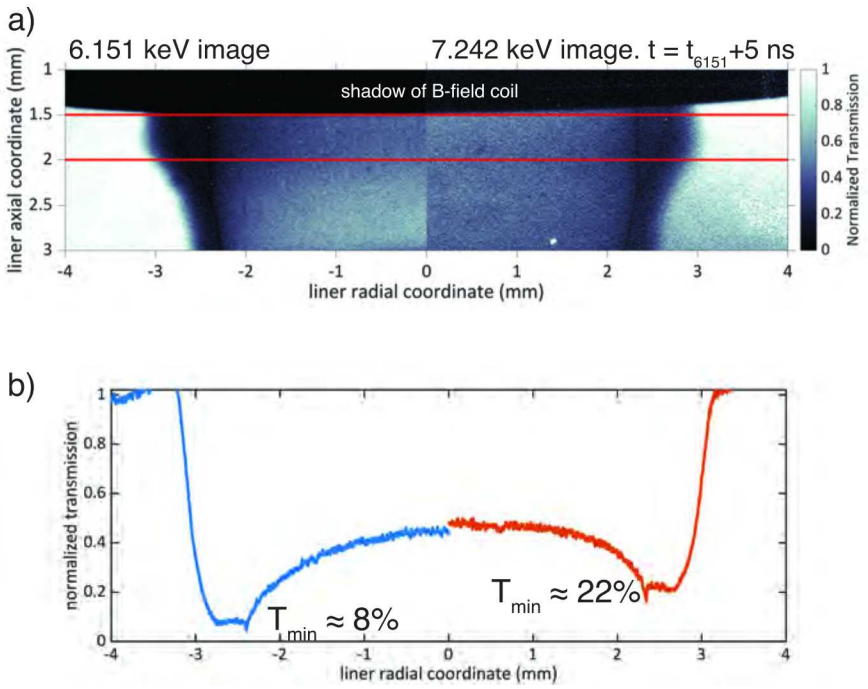

FIG. 7. Two-color radiographs taken at an early time during an imploding 'thick-ends' liner at Z. a) the left radiograph was taken with 6.151-keV x-rays, the right radiograph was taken 5 ns later with 7.242 keV. b) shows a lineout of the area marked by the red lines in a). The limb transmission of the 7.2-keV x-rays is about a factor of three better than the 6.2-keV transmission.

neither the crystal nor the return apertures were misaligned, leaving the x-ray source as the culprit. Post-shot ray-tracing simulations showed that an x-ray source movement of about 1 mm or more in vertical direction (up) could reproduce the experimental radiographs.

The x-ray source (laser targets) are Co foils glued onto 3-mm diameter Al disks, which in turn are held in place by gravity in a cutout area on a larger Al laser target holder. Fig. 8a shows two Mn foils on their Al disks in the laser target holder. This configuration has worked well for many years without any issues or clipped radiographs. However, Mn and the Al disk are anti-ferromagnetic and not affected by the fringe magnetic fields at Z, whereas Co is strongly ferromagnetic. The experiment in Fig. 7 used an applied magnetic field from Helmholtz coils[25]. The fringe magnetic field strength from the field coils can reach 0.5 T or more near the laser targets at an early time in the current discharge. The magnetic force vector at the target location points in a direction that pulls the Co targets up and towards the Z center. As a result, the entire Al disk flips into an almost vertical orientation, which leads to a vertical shift of the apparent x-ray source when the laser hits and also to a reduced

laser-to-x-ray energy conversion.

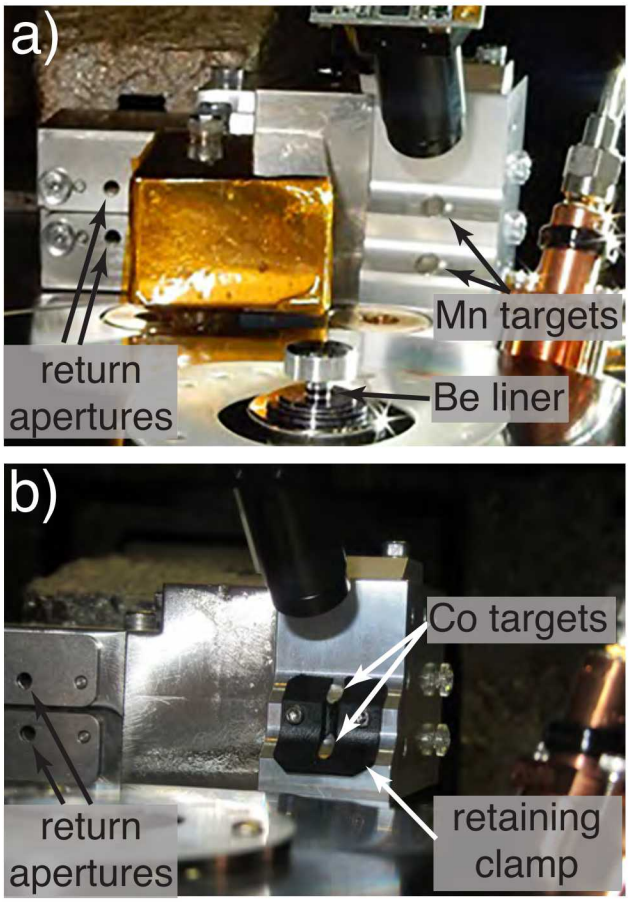

FIG. 8. Comparison of the laser target block without (a) and with (b) the retaining clamp. The clamp is necessary for shots with Co targets, because fringe magnetic fields during the Z discharge pull the ferromagnetic Co foils out of their nominal positions.

To eliminate Co target movement in the following shots, a retaining clamp was designed and manufactured in-house with selective laser sintering. Fig. 8b shows the re-designed laser target block with the retaining clamp.

Fig. 9 shows two 7.2-keV radiographs of a Z shot using the clamp. The images are well exposed, have a homogeneous flat field distribution, and exhibit a high contrast. The total laser energies were 1.2 kJ in the first frame and 1 kJ in the second frame; the distributions of energy into the prepulse and main pulse are shown in the picture. Both images have a photon fluence of 5 to 6 photons/μm^2, which is amongst the highest fluence radiographs recorded at Z.

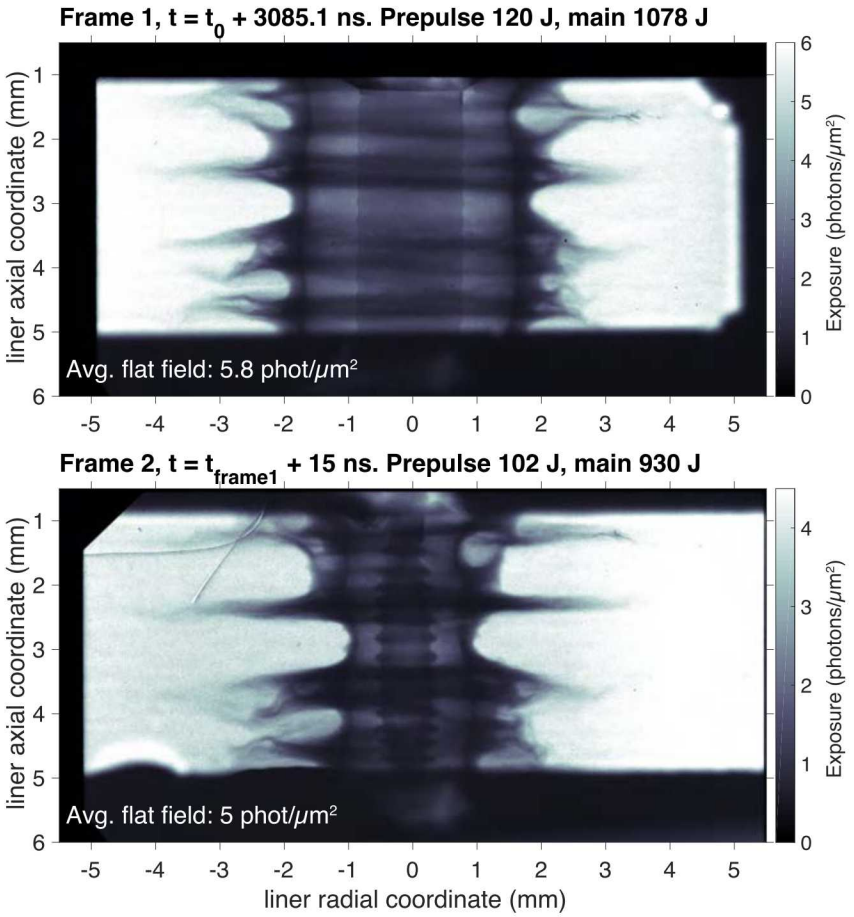

FIG. 9. Two-frame 7.242 keV radiographs of an imploding liner with sinusoidal on-axis rod. Frame 1 was taken 3085.1 ns after start of the Z discharge, Frame 2 was taken 15 ns later. Both images exhibit a high contrast and transmission through the liner. The flat field image brightness outside the liner region is 5 to 6 photons/μm^2.

The initial liner diameter was much larger than a standard MagLIF-liner, resulting in a high areal density. Due to the higher-than-normal density the 7.2-keV system was fielded for improved visibility of the inner rod compared to the 6.2-keV backlighter. The Be liner in this experiment was filled with liquid D_2 and had an inner on-axis rod with sinusoidal perturbations. In the 15 ns between frame 1 and frame 2, both the liner and the inner rod are compressed, the amplitude of the rod surface modulations increases, and an axial asymmetry in the compression is evident. The goal of the radiographs shown in Fig. 9 was not to achieve the highest compression, but to see the evolution of the on-axis rod surface modulations during the deceleration phase nearing stagnation. The radiographs shown in

the figure were taken at C_R of about 4-5. In subsequent campaigns, 7.2-keV radiographs with C_R up to about 20 have been measured. Data analysis is still ongoing and results will be published in future articles.

A comparison of 14 Z experiments, where seven experiments used the 6.2 keV backlighter system and seven used the new 7.2 keV backlighter system, for a total of 28 radiographs, showed that on average the 7.2 keV radiographs ($\approx 7\,\text{photons}/\mu\text{m}^2$) are about 1.7 times brighter than the 6.2 keV radiographs ($\approx 4\,\text{photons}/\mu\text{m}^2$). One notable difference between the 6.2 and 7.2 keV systems is that the 6.2 keV backlighter uses the intercombination line and the 7.2 keV backlighter uses the resonance line of the He-like spectrum. The efficiency for imaging may depend on the optical depth of the line, which varies between the resonance and intercombination lines. Furthermore, surrounding hardware or dynamic processes in a Z experiment may adversely or positively affect the laser-plasma interaction and x-ray generation during the shot. For example, the 7.2 keV x-rays have less attenuation through the light-blocking filters, Be debris shields or Be return current can than 6.2-keV x-rays. Potential parasitic radiation emission at an early time during the Z discharge could lead to preheat of the target, crystal or both, affecting the efficiency of the imaging system. These factors change from experiment to experiment and are very hard if not impossible to predict.

VI. SUMMARY

A 7.242-keV backlighter system using a spherical Ge (335) crystal and the Co He_α resonance line has been developed and fielded at the Z Pulsed Power Facility at Sandia National Laboratories, NM, USA. The crystal and x-ray source parameters were chosen after a systematic evaluation was performed to find spectral-line and spherical-crystal matches suitable for high-resolution imaging with a Bragg angle near 83°. The 7.242-keV backlighter system operates at a Bragg angle of 82.8°, which is compatible with the existing 1.865-keV (83.9°) and 6.151-keV (83.19°) backlighter systems. Laser-only tests at the Z-Backlighter facility confirmed that the new backlighter system meets the requirements with an image brightness of more than 2 photons/μm^2 and spatial resolution of better than 15 μm (10%-90% knife edge width). The first dynamic radiographs at the Z facility revealed that fringe magnetic fields during an early time of the Z current discharge can pull the Co targets out of their

nominal positions, which results in compromised radiographs that have a poor exposure as well as a vertical gradient. This issue was eliminated by adding a retaining clamp to the laser target holder. Subsequent Z shots produced successful 7.242-keV radiographs with a high contrast and transmission through the liner, a homogeneous flat field and an image brightness above 5 photons/μm^2. This new 7.242-keV backlighter system has now been added as a standard diagnostic at Z and is available to experimenters.

VII. ACKNOWLEDGMENTS

The authors would like to thank the Sandia MagLIF, Z operations, Z-Beamlet, target fabrication, Z center section, Z diagnostics, CMDAS, Lab 101, and gas fill teams. Sandia National Laboratories is a multimission laboratory managed and operated by National Technology and Engineering Solutions of Sandia, LLC., a wholly owned subsidiary of Honeywell International, Inc., for the U.S. Department of Energy's National Nuclear Security Administration under contract DE-NA-0003525.

REFERENCES

[1]J.A. Koch, O.L. Landen, T.W. Barbee, P. Celliers, L.B. Da Silva, S.G. Glendinning, B.A. Hammel, D.H. Kalantar, C. Brown, J. Seely, G.R. Bennett, and W. Hsing, "High-energy x-ray microscopy techniques for laser-fusion plasma research at the National Ignition Facility", Applied Optics **37**, 1784 (1998).

[2]T.A. Pikuz, A.Y. Faenov, I.Y. Skobelev, A.I. Magunov, M. Sanchez del Rio, L. Alianelli, G. Baldacchini, F. Flora, S. Bollanti, P. Di Lazzaro, D. Murra, G. Tomassetti, A. Ritucci, A. Reale, L. Reale, M. Francucci, S. Martellucci, and G. Petrocelli, "High efficient X-ray imaging and backlighting schemes based on the spherically bent crystals", Proc. SPIE **5196**, 362 (2004).

[3]G. R. Bennett, D. B. Sinars, D. F. Wenger, M. E. Cuneo, R. G. Adams, W. J. Barnard, D. E. Beutler, R. A. Burr, D. V. Campbell, L. D. Claus, and et al., "High-brightness, high-spatial-resolution, 6.151 kev x-ray imaging of inertial confinement fusion capsule implosion and complex hydrodynamics experiments on Sandia's Z accelerator (invited)," Review of Scientific Instruments **77**, 10E322 (2006).

[4]D. B. Sinars, G. R. Bennett, D. F. Wenger, M. E. Cuneo, D. L. Hanson, J. L. Porter, R. G. Adams, P. K. Rambo, D. C. Rovang, and I. C. Smith, "Monochromatic x-ray imaging experiments on the Sandia National Laboratories Z facility (invited)," Review of Scientific Instruments **75**, 3672 (2004).

[5]Y. Aglitskiy, M. Karasik, A.L. Velikovich, V. Serlin, J.L. Weaver, A.J. Schmitt, S.P. Obenschain, N. Metzler, S.T. Zalesak, J.H. Gardner, J. Oh, and E.C. Harding, "Stability of a Shock-Decelerated Ablation Front", Phys. Rev. Lett. **103** 085002 (2009).

[6]C. Stoeckl, M. Bedzyk, G. Brent, R. Epstein, G. Fiksel, D. Guy, V. N. Goncharov, S. X. Hu, S. Ingraham, D. W. Jacobs-Perkins, R. K. Jungquist, F. J. Marshall, C. Mileham, P. M. Nilson, T. C. Sangster, M. J. Shoup III, and W. Theobald, "Soft x-ray backlighting of cryogenic implosions using a narrowband crystal imaging system (invited)", Review of Scientific Instruments **85**, 11E501 (2014).

[7]W. Theobald, A.A. Solodov, C. Stoeckl, K.S. Anderson, F.N. Beg, R. Epstein, G. Fiksel, E.M. Giraldez, V.Yu. Glebov, H. Habara, S. Ivancic, L.C. Jarrott, F.J. Marshall, G. McKiernan, H.S. McLean, C. Mileham, P.M. Nilson, P.K. Patel, F. Perez, T.C. Sangster, J.J. Santos, H. Sawada, A. Shvydky, R.B. Stephens, M.S. Wei, "Time-resolved compression of a capsule with a cone to high density for fast-ignition laser fusion", Nature Commun. **5**, 5785 (2014).

[8]Q. Yang, D. Liu, J. Mu, X. Huang, J. Dan, X. Xie, W. Deng, S. Feng, M. Wang, Y. Ye, Q. Peng, and Z. Li, "X-ray backlighting of imploding aluminium liners on PTS facility", Rev. Sci. Instrum. **87**, 093706 (2016).

[9]M. E. Savage, K. R. Lechien, M. R. Lopez, B. S. Stoltzfus, W. A. Stygar, D. S. Artery, J. A. Lott, and P. A. Corcoran, *Status of the Z pulsed power driver*, IEEE Pulsed Power Conference, pp. 983–990, (2011).

[10]R. McBride, S. Slutz, C. Jennings, D. Sinars, M. Cuneo, M. Herrmann, R. Lemke, M. Martin, R. Vesey, K. Peterson, and et al., "Penetrating radiography of imploding and stagnating beryllium liners on the z accelerator," Physical Review Letters **109**, 135004 (2012).

[11]D. Sinars, S. Slutz, M. Herrmann, R. McBride, M. Cuneo, K. Peterson, R. Vesey, C. Nakhleh, B. Blue, and K. Killebrew, "Measurements of magneto-rayleigh-taylor instability growth during the implosion of initially solid al tubes driven by the 20-ma, 100-ns z facility," Physical Review Letters **105**, 185001 (2010).

[12]T. J. Awe, C. A. Jennings, R. D. McBride, M. E. Cuneo, D. C. Lamppa, M. R. Martin, D. C. Rovang, D. B. Sinars, S. A. Slutz, A. C. Owen, and et al., "Modified helix-like instability structure on imploding z-pinch liners that are pre-imposed with a uniform axial magnetic fielda)," Physics of Plasmas **21**, 056303 (2014).

[13]T. J. Awe, R. D. McBride, C. A. Jennings, D. C. Lamppa, M. R. Martin, D. C. Rovang, S. A. Slutz, M. E. Cuneo, A. C. Owen, D. B. Sinars, and et al., "Observations of modified three-dimensional instability structure for imploding z-pinch liners that are premagnetized with an axial field." Physical Review Letters **111**, 235005 (2013).

[14]T. J. Awe, K. J. Peterson, E. P. Yu, R. D. McBride, D. B. Sinars, M. R. Gomez, C. A. Jennings, M. R. Martin, S. E. Rosenthal, D. G. Schroen, and et al., "Experimental demonstration of the stabilizing effect of dielectric coatings on magnetically accelerated imploding metallic liners," Physical Review Letters **116**, 065001–5 (2016).

[15]K. J. Peterson, T. J. Awe, E. P. Yu, D. B. Sinars, E. S. Field, M. E. Cuneo, M. C. Herrmann, M. Savage, D. Schroen, K. Tomlinson, and et al., "Electrothermal instability mitigation by using thick dielectric coatings on magnetically imploded conductors," Physical Review Letters **112**, 135002 (2014).

[16]A. B. Sefkow, S. A. Slutz, J. M. Koning, M. M. Marinak, K. J. Peterson, D. B. Sinars, and R. A. Vesey, "Design of magnetized liner inertial fusion experiments using the z facilitya)," Physics of Plasmas **21**, 072711 (2014).

[17]S. A. Slutz, M. C. Herrmann, R. A. Vesey, A. B. Sefkow, D. B. Sinars, D. C. Rovang, K. J. Peterson, and M. E. Cuneo, "Pulsed-power-driven cylindrical liner implosions of laser preheated fuel magnetized with an axial field," Physics of Plasmas **17**, 056303 (2010).

[18]M. R. Gomez, S. A. Slutz, A. B. Sefkow, K. D. Hahn, S. B. Hansen, P. F. Knapp, P. F. Schmit, C. L. Ruiz, D. B. Sinars, E. C. Harding, and et al., "Demonstration of thermonuclear conditions in magnetized liner inertial fusion experiments)," Physics of Plasmas **22**, 056306–10 (2015).

[19]P. Rambo, J. Schwarz, M. Schollmeier, M. Geissel, I. Smith, M. Kimmel, C. Speas, J. Shores, D. Armstrong, J. Bellum, and et al., "Sandia's Z-backlighter laser facility," Proc. of SPIE, **10014**, 100140Z (2016).

[20]G. R. Bennett, I. C. Smith, J. E. Shores, D. B. Sinars, G. Robertson, B. W. Atherton, M. C. Jones, and J. L. Porter, "220 ns interframe time 2-frame 6.151 kev x-ray imaging on the recently upgraded z accelerator: A progress report," Review of Scientific Instruments

79, 10E914–4 (2008).

[21]D. B. Sinars, G. R. Bennett, D. F. Wenger, M. E. Cuneo, and J. L. Porter, "Evaluation of bent-crystal x-ray backlighting and microscopy techniques for the sandia z machine," Applied Optics **42**, 4059–4071 (2003).

[22]M. Geissel, C. Cox, M. Schollmeier, J. E. Shores, I. C. Smith, C. S. Speas, and J. L. Porter, *Optimization of X-ray backlighting for experiments on Z* (2013), IEEE Pulsed Power Conference, 2013

[23]M. S. Schollmeier and G. P. Loisel, "Systematic search for spherical crystal x-ray microscopes matching 1-25 kev spectral line sources." Review of Scientific Instruments **87**, 123511 (2016).

[24]J. P. Chittenden, S. V. Lebedev, C. A. Jennings, S. N. Bland, and A. Ciardi, "X-ray generation mechanisms in three-dimensional simulations of wire array z-pinches," Plasma Physics and Controlled Fusion **46**, B457–B476 (2004).

[25]D. C. Rovang, D. C. Lamppa, M. E. Cuneo, A. C. Owen, J. McKenney, D. W. Johnson, S. Radovich, R. J. Kaye, R. D. McBride, C. S. Alexander, and et al., "Pulsed-coil magnet systems for applying uniform 10-30 T fields to centimeter-scale targets on Sandia's Z facility," Rev. Sci. Instrum. **85**, 124701 (2014).

[26]L.E. Ruggles, J.L. Porter, P.K. Rambo, W.W. Simpson, M.F. Vargas, G.R. Bennett, and I.C. Smith, "Measurements of 4–10 keV x-ray production with the Z-Beamlet laser", Rev. Sci. Instrum. **74**, 2206 (2003).

[27]M. S. Schollmeier, M. Geissel, J. E. Shores, I. C. Smith, and J. L. Porter, "Performance of bent-crystal x-ray microscopes for high energy density physics research." Applied Optics **54**, 5147–5161 (2015).

[28]M. S. d. Rio and R. J. Dejus, "XOP v2. 4: recent developments of the x-ray optics software toolkit," Proc. of SPIE **8141**, 814115 (2011).

[29]D. B. Sinars, G. R. Bennett, M. C. Herrmann, I. C. Smith, C. S. Speas, L. E. Ruggles, and J. L. Porter, "Enhancement of x-ray yield from the Z-Beamlet laser for monochromatic backlighting by using a prepulse," Review of Scientific Instruments **77** (2006).

[30]T. Ao, E. C. Harding, J. E. Bailey, G. Loisel, S. Patel, D. B. Sinars, L. P. Mix, and D. F. Wenger, "Relative x-ray collection efficiency, spatial resolution, and spectral resolution of spherically-bent quartz, mica, germanium, and pyrolytic graphite crystals," Journal of Quantitative Spectroscopy and Radiative Transfer **144**, 92–107 (2014).

[31]Thick-ends liner design by A.B. Sefkow (Rochester University, Rochester, NY, USA).